Research article

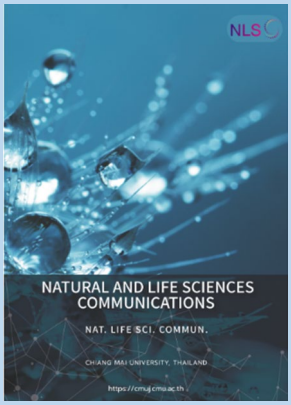

Editor:
Laongnuan Srisombat,
Chiang Mai University, Thailand

Article history:
Received: February 27, 2024;
Revised: May 16, 2024;
Accepted: May 17, 2024;
Online First: June 6, 2024
https://doi.org/10.12982/NLSC.2024.035

Corresponding author:
Irfan Navabshan
E-mail: irfan@crescent.education

Fabrication of Silver Nanoparticles Using *Acalypha paniculata* Extract, AI-Based Interaction Analysis and Its Activity Explication

Elumalai A. and Irfan Navabshan*

Crescent School of Pharmacy, B.S. Abdur Rahman Crescent Institute of Science and Technology, GST Road, Vandalur, Chennai, Tamilnadu, India-600048.

ABSTRACT

This study showcases eco-friendly silver nanoparticle synthesis using Acalypha paniculata herb and its biological activity. Artificial Intelligence (AI) tools are used to analyze the interaction between phytoconstituent and silver ion to find the capping and nanoparticle fabricating phytoconstituents. Ethanolic extract was added to silver nitrate solution and irradiated under sunlight until the formation of silver nanoparticles. These particles were sedimented, characterised by spectral technique and biological activity was measured. Finally, a Computational simulation algorithm was used to visualize the interactions of phytoconstituent and silver nanoparticles. Ultra Violet (UV)-visible spectrum revealed a visible peak at 420nm in the brownish solution, Dynamic Light Scattering (DLS) size of 54.7nm, spherical crystalline morphology of the nanoparticle by Transmission Electron Microscope (TEM) and X-Ray Diffraction (XRD) analysis. The synthesized silver nanoparticle antagonised Escherichia coli, and Bacillus cereus and showed the Minimum Inhibitory Concentration (MIC) of 65 µg/mL, and 78 µg/mL respectively and Minimum Bacterial Concentration (MBC) of 52.5 µg/mL for B.cereus and 61.5µg/mL for *E.coli*. The 2,2-diphenyl-1-picrylhydrazyl (DPPH) free radicals IC_{50} was found to be 97.414 µg/mL and it revealed the dose-dependent antioxidant activity of phyto-capped silver particles. The cytotoxicity of fabricated nanoparticles was studied on Vero cells and the results indicate that IC_{50} of 47.28 µg/mL. Furthermore, an AI-based study concludes that Alloaromadendrene adsorbed highly by the Silver (Ag) ion compared to the nitrate with an affinity of -30.6755 kcal/mol. This research introduces an innovative, cost-effective method for stable *Acalypha paniculata* Silver Nanoparticles (AP-AgNPs) fabrication, crucial for diverse biomedical uses.

Keywords: *Acalypha paniculata*, Silver nanoparticles, Antibacterial activity, Antioxidant, cytotoxicity.

Citation: Elumalai, A. and Irfan, N. 2024. Fabrication of silver nanoparticles using *Acalypha paniculata* extract, AI-based interaction analysis and its activity explication. Natural and Life Sciences Communications. 23(3): e2024035.

INTRODUCTION

Nanotechnology involves the creation of particles in the range of 1 to 100 nm. Recent advancements in synthesizing nanoparticles from various materials have opened up new avenues for research and application. The nanoparticle's size and shape are dependent on the chosen synthesis method, whether chemical, physical, or biological. Among that, chemical and physical synthesis methods are frequently linked to environmental concerns due to their reliance on toxic organic solvents, harmful by-product generation, and high energy consumption.

To surmount these challenges, a new technique has emerged as an alternative method: green synthesis, which is eco-friendly, cost-effective, and simple to carry out, while also having the potential to produce large quantities of nanoparticles (Ponsanti et al., 2020; Vanlalveni et al., 2021; Flieger et al., 2022). Despite these advantages, the application of green synthesis methods still faces limitations, particularly in terms of scalability and control over nanoparticle properties, necessitating further exploration and refinement.

Numerous studies have shown that plants have the potential for green production of metal nanoparticles owed to the existence of secondary metabolites like alkaloids, terpenoids, phenols, essential oils, and flavonoids (Wang et al., 2021; Kalaiyan et al., 2023; Sheik Aliya et al., 2023). These metabolites serve as reducing and capping agents during metallic nanoparticle formation. Plant extracts that contain nanoparticles poised of different metals have revealed assorted biological activities. Among these nanoparticles, silver nanoparticles are particularly significant owing to their exceptional properties such as good conductivity, chemical inertness, and catalytic ability, as well as their potent antimicrobial, antiviral, antifungal, anti-arthritic, and anti-inflammatory activities (Khojasteh-Taheri et al., 2023; Kindnew Demssie Dejen et al., 2023). Modification of crude plant extracts with metal nanoparticles has shown enhanced activity when compared to crude extracts alone.

This research aims to explore the green synthesis of silver nanoparticles using *Acalypha paniculata* leaf extract and investigate their potential biological activities. Specifically, the objectives include optimizing the synthesis process, characterizing the synthesized nanoparticles, elucidating the mechanisms of nanoparticle formation through computational analysis, and evaluating their biological properties such as antimicrobial and antioxidant activities. By achieving these objectives, this study seeks to contribute to the advancement of sustainable nanotechnology and validate the traditional applications of *Acalypha paniculata* in modern scientific contexts.

Acalypha paniculata is a member of the *Euphorbiaceae* family, predominantly found in the Parvathamalai hills of the Eastern Ghats in Tamilnadu. In local, the plant is called a9s kothu kuppameni. The different parts of *Acalypha paniculata* have been traditionally used for their medicinal properties and health benefits (Musa et al., 2000; Iniaghe et al., 2008). In folklore medicine, the leaves are applied in dressing wounds and arthritis. This herbaceous plant can grow to be 0.5 to 1 meter tall at various altitudes. The aerial parts of the plant are often used in decoctions for pain relief from inflammation caused by fractures and arthritis (Djacbou et al., 2014). To advance and prove this concept of the traditional application of A. paniculata, two major works was performed in this study. At first, a photochemical reaction was used to produce silver nanoparticles from the leaf extract of A. paniculata (AP-AgNPs). Secondly, computational interpretation was performed between the phytoconstituents of A. paniculata and silver ion to analyze the formation of nanoparticles. Additionally, biological activities such as free radical scavenging, MIC, MBC, and cell cytotoxicity studies were performed and interpreted computationally as well as experimentally.

MATERIALS AND METHODS

Preparation of the extract and silver nanoparticle synthesis

The collection of the aerial parts of *Acalypha paniculata* was performed from the Parvathamalai hills situated in the state of Tamilnadu in India. The authentication and identification of the plant were conducted by the Department of Pharmacognosy at the Siddha Central Research Institute (CCRS), which is under the Ministry of Ayush, Government of India, which is situated in Chennai 600106 (Ref: H12092201S).

The leaves of *A. paniculata* were harvested and cleaned with distilled water to eliminate any impurities. To prepare the leaves extract, air-dried leaves weighing 45 grams were finely powdered using a blender and filled in the Soxhlet apparatus to extract phytoconstituent of AP for 8 hours. The 200mL of ethanol was taken in RBF and the temperature range was fixed and maintained at 55°C ± 5°C throughout the 8-hour process. The final extract was meticulously preserved for the ensuing amalgamation of silver nanoparticles. A solution of 1mM silver nitrate was prepared by mixing 0.016g of silver nitrate and 100 mL of water for the optimization of AgNPs formation. Ten mL of silver nitrate solution was taken in 5 test tubes and ethanolic extract of *A. paniculata* solution was added in the concentration of 5µL to 25µL. Furthermore, the solution was irradiated in sunlight to observe the formation of Ag nanoparticles (Irfan and Puratchikody, 2012; Gunashekar Kalvakunta Subramanyam et al., 2023; Hafiz Saad Ahmad et al., 2023). The optimized final solution was prepared on a large scale and separated using a high-speed centrifuge at 10,000 rpm. The sedimented nanoparticles were vacuum freeze-dried and stored for further usage.

Characterization of silver nanoparticle

UV spectroscopy

A spectra module in a UV-visible spectrometric (UV-1900 Sumatzu) system was used to scan the complete range from 200-800 nm radiation to find the λmax of the extract and silver nanoparticle solution. A dual-beam spectrophotometer was performed spectral analysis at normal temperature and the instrument ran at a spatial resolution of 1 nm and a scanning rate of 200 nm/min. The scan speed was set as slow with three repetition runs and the detection of peak threshold of 0.001.

FT-IR

To study the functional group analysis by vibrational changing of atomistic level for the formed nanoparticle and ethanolic extract was performed in Shimadzu IR-tracer100 instrument. Dried AgNPs powder was mixed with KBr in the ratio of 1:100 in mortar and hydraulic pressure was used to make the thin pellet. This pellet was fixed in the dia and IR transmission range of 4000-800 cm^{-1} was passed. The maximum CO_2 peaks were smoothened to find the better peaks. Final spectra were generated and interpreted.

Dynamic light scattering (DLS) and ZETA potential

The Zetasizer Nano ZS instrument from Malvern Instruments Ltd., UK, was utilized to examine the distribution size of AP-AgNPs. By capitalizing on the fluctuations in light scattering intensity resulting from the Brownian motion of particles, this device effectively examines and analyses the distribution of particle sizes. Throughout the analysis, significant data points were identified, including the peak values within the hydrodynamic diameter distribution, the average hydrodynamic diameter of the particles, and the polydispersity index (PdI). The PdI quantifies the extent of variability in the particle size distribution,

ranging from 0 to 1. A value of 0 signifies a uniform distribution, while a value of 1 suggests a diverse distribution. A one-minute temperature equilibration period at 25°C was used for the measurements, which were carried out in triplicate. The obtained results were summarized and presented in Table 1, providing a comprehensive overview of the size distribution of AP-AgNPs. The determination of zeta potential is important in evaluating the dispersion, surface charge, and stability of nanoparticles. The AP-AgNPs powder was dispersed in distilled water for 30 minutes using an ultrasonicator. The range of zeta potential for stable suspensions is between 20 and 60 mV. The dispersions are prone to aggregation when the zeta potential drops below this range because of the van der Waals attraction forces between each particle. On the other hand, a higher zeta potential results in particle repulsion, leading to stable particles with a low propensity to aggregate.

TEM

A JEOL-2100 plus microscope running at 200 kV of acceleration was used for the analysis of dimensions and morphology of the synthesized AP-AgNPs in High-resolution Transmission Electron Microscopy (TEM). The sample was prepared by dispersing it in ethanol at an appropriate concentration. A carbon-coated copper grid was carefully placed with a small drop of the resulting solution. The film was allowed to deposit on the TEM grid for 2 minutes, after which any excess solution was eliminated using blotting paper. Before the measurement, the grid was allowed to dry for a whole night at room temperature while operating at 60 kV. The TEM images scale bar was used to calibrate the software.

XRD

The crystal structure of the AP-AgNPs was analyzed by X-ray diffraction (XRD) using a Cu Kα radiation source (λ = 1.540562 Å). The XRD analysis was performed for a duration of 2 hours at 30–40 kV and 15 mA. The measurements were taken on a 20-degree scale with a step size of 0.02 degrees.

Computational mechanism prediction of nanoparticle formation and stabilization

The mechanism of silver ion reduction and caping phytoconstituent was predicted using the classical molecular mechanic tools using material studio software from the BIOVIA. In this AI-based work, 18 phytoconstituents of AP, Silver Nitrate, and water molecules are given as input in the forcite minimization. The Condensed-phase Optimized Molecular Potentials for Atomistic Simulation Studies (COMPASS) force field was set and the electrostatic and van der Waals by atom-based were summated.

The Amorphous Cell algorithm builds three-dimensional (3D) periodic structures with the phytoconstituents of AP, Silver Nitrate and water molecule system in a Monte Carlo fashion and minimizing close contacts between atoms. 18 components of AP were loaded in the composition box for cell construction. Finally, the Blends module aids in forecasting the interaction of all 18 phytoconstituents with water and silver nitrate. The blend task is fixed as mixing and the quality of work is set as fine. All the molecules are loaded into the input table and the role of 14 components of AP is fixed as Screen. This unique technique is used to predict the caping phytoconstituent of AP which is responsible for the formation of nanoparticle and particle stabilization.

Antibacterial assay (Agar well diffusion (AWD) assay)

The AWD method was employed to assess the antibacterial efficacy of *A. paniculata* ethanolic extract and AP-AgNPs against a range of bacteria, encompassing Gram-positive strains like *Staphylococcus aureus* and *Bacillus cereus,* as well as Gram-negative strains such as *Pseudomonas fluorescens* and

Escherichia coli (Sarinya Poadang et al. 2017; Eli Rohaeti and Anna Rakhmawati. 2022; Linima et al, 2023; Usa Sukkha et al. 2023). To conduct the experiment, pure cultures of the microorganisms were acquired by subculturing them on a nutrient agar medium, followed by incubation at 37°C for a duration of 24 hours. Fresh overnight cultures of the bacteria were then used to inoculate sterile swabs, which were subsequently spread on Mueller Hinton agar (MHA) plates. Afterward, wells were created in the agar using a sterile instrument, and the extract and AP-AgNPs were added to separate wells. Following the addition of the test substances, the MHA plates were allowed to stand for 20 minutes, facilitating the diffusion of the extract or AP-AgNPs into the surrounding agar. This allowed the antibacterial activity of the extract and AP-AgNPs to take effect, inhibiting the growth of the bacteria. A prominent approach for evaluating a substance's antibacterial capabilities is the AWD method, which enables the observation and measurement of inhibition zones around the wells, indicating the effectiveness of the tested materials against the bacteria. Wells with a diameter of 6 mm were created on the MHA plates containing the bacterial lawn. Two different concentrations 10, 20µL of Acalypha paniculata ethanolic extract and AP-AgNPs separately were filled in the wells. Chloramphenicol (10 µg/mL) was used as a reference standard.

Once the agar plates were prepared with the Acalypha paniculata ethanolic extract and AP-AgNPs, 24 hrs incubation condition was set at a temperature of 37°C and left undisturbed for a period of 24 hours. This incubation period allowed the bacteria to multiply and the extract's and AP-AgNPs' antibacterial activities to become apparent. The plates were examined and the widths of the inhibition zones surrounding the wells were measured after the incubation period. This measurement provided quantitative information on the extent of bacterial growth inhibition caused by the extract and AP-AgNPs. To ensure reliable and accurate results, the experiments were conducted in triplicate. This repetition of the experiment helps account for any potential variations and provides a more robust evaluation of the antibacterial effectiveness of the extract and AP-AgNPs. To maintain proper laboratory hygiene and prevent contamination, appropriate disposal procedures were followed for the microbial cultures. This involved using an autoclave, a device that utilizes high pressure and temperature to sterilize and inactivate the microorganisms, thus ensuring their safe disposal.

Evaluation of MIC and MBC

To determine AP-AgNPs' Minimum Inhibitory Concentration (MIC) value for Bacillus cereus, the broth microdilution method was exploited. Fresh sterilized Brain Heart Infusion (BHI) media of 100 µL were added in round-bottom 96-well microtiter plate. A stock containing 100 µl of 1 mg/mL concentrated AP-AgNPs was added to the first well to establish a serial dilution. The subsequent wells were then subjected to serial dilutions, resulting in a gradient of AP-AgNPs concentrations in the plate. Immediately after the serial dilution, Bacillus cereus culture with a concentration of 10^6 CFU/mL (Colony Forming Units per millilitre) was added to each well, introducing the bacteria to different concentrations of AP-AgNPs. A well without the addition of AP-AgNPs but containing only the bacterial culture served as the positive control, while another well with only the media served as the negative control. The plates were examined and the widths of the inhibition zones surrounding the wells were measured after the incubation period. Subsequently, optical density (OD) readings at a wavelength of 600 nm were taken using a 96-well ELISA plate reader. These readings provided information on the growth of the bacteria in the existence of different AP-AgNPs concentrations. In order to determine the percentage of cell death, an equation was employed, considering the OD readings acquired. By analyzing the percentage of cell death at various AP-AgNPs concentrations, the MIC value of AP-AgNPs against Bacillus cereus could

be determined. After that, the microtiter plates were kept at 37°C overnight to promote bacterial growth. To assess the bacterial growth inhibition, the cell death percentage was determined using the equation presented below:

$$Bacterial\ growth\ (\%) = \frac{(OD\ control - OD\ sample)}{OD\ control} \times 100$$

In this equation, the OD control refers to the optical density of the control wells, which contained the bacterial culture without the addition of AP-AgNPs. On the other hand, the OD sample represents the optical density of the sample wells, which contained the bacterial culture exposed to different concentrations of AP-AgNPs.

To measure the MBC (minimum bactericidal concentration), A 10 µL volume of sample from wells with the MIC concentration and higher concentrations was transferred onto a blood agar medium and incubated for 24 hours. After incubation, the MBC was determined as the concentration at which no visible bacterial growth was detected on the blood agar medium. This concentration represents the lowest concentration of AP-AgNPs or extract that not only inhibits bacterial growth (MIC) but also completely eradicates the bacteria. To ensure reliable and accurate results, each step of the process was repeated three times.

DPPH assay

To evaluate the DPPH radical scavenging activities of the extract and AP-AgNPs, we employed a method similar to the one outlined by Luhata et al., 2022. Five different doses (10, 20, 30, 40, and 50 µg/mL) of AP-AgNPs was taken. Each concentration was mixed with 1 mL of a 0.004% DPPH solution. As a control, we combined 1 mL of DPPH with 1 mL of methanol. Ascorbic acid was employed as standard. Subsequently, the absorbance of the solutions was measured at a wavelength of 517 nm using a UV-visible spectrophotometer.

***In-vitro* cytotoxic assay by MTT assay**

To assess the cytotoxicity of AP-AgNPs against Vero cells (African green monkey kidney cells) the MTT assay was performed. The cell was sourced from the NCCS, Pune, and cultured in Dulbecco's Modified Eagle (DME) Medium supplemented with 10% fetal bovine serum (FBS) and 1% antimycotic solution. The cells were detached using a trypsin-EDTA solution. A cell density of $1x10^5$ cells/mL was seeded and incubated at 37°C in 96-well plates, with 100% relative humidity, 95% air and 5% CO_2, to facilitate cell attachment. Different concentrations (1-512 µg/ml) of the extracts were prepared and added to the wells, which already contained 100µl of the culture medium. The plate temperature was set at 37°C in an incubator and kept undisturbed for 48 hours. Non-treated cells were used as the control, and all experiments were conducted in triplicate. Following a 48-hour incubation period, each well was added 15 µL of Phosphate Buffer Saline containing MTT (5 mg/mL) and again incubated at the same condition. Subsequently, the medium with MTT was aspirated, and the resulting formazan crystals were dissolved in 100µL of DMSO. The absorbance was then measured at 570 nm using a microplate reader. The cell survival graph was generated to determine the IC_{50} value.

The cell inhibition (%) was measured using the equation of

$$Percentage\ of\ Cell\ Inhibition = \frac{A - Ao}{AO} \times 100$$

Where, A – Absorbance of sample, *AO* – absorbance of control

Apoptotic cell death analysis by fluorescence microscopy

About 1µL of a mixture containing AO/EtBr stain was added to Vero cells suspension against IC_{50} dose of AP-AgNPs. The stained cell suspensions were then applied onto clean microscopic slide. Following the pre-treatment, the cell lines were rinsed using PBS (pH 7.2) and subjected to staining with AO/EtBr. Subsequently, the cells were incubated for 2 minutes in a sterile environment and examined in a fluorescence microscope.

RESULTS

Synthesis of silver nanoparticles

Scientific research has looked closely at the creation of AgNPs using extracts from different plant components. In these experiments, when an aqueous solution of silver nitrate is mixed with *A. paniculata* ethanolic leaf extracts, a distinct colour change in the solution was observed after the sunlight irradiation. Initially, the solution appears pale yellow, but as the reaction progresses, it gradually transforms into a dark brown or reddish-brown colour (Figure 1) The optimization work shows that the addition of 5µL extract in the 1mmol silver nitrate solution produced fast AgNPs within 10 minutes under sunlight radiation. The addition of a higher (15µL) extract with the silver nitrate solution produced precipitation due to the aggregation mechanism.

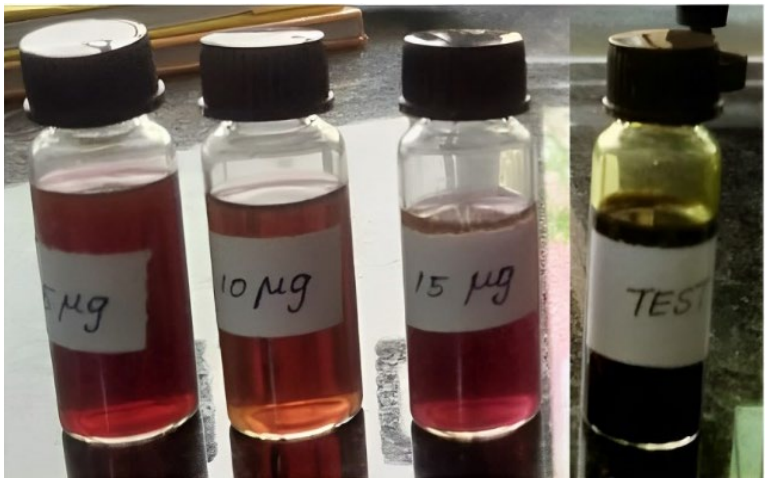

Figure 1. Formation of AgNPs in different extract concentrations.

Characterization of silver nanoparticles

The result of the UV-visible spectroscopy scan revealed a distinct surface plasmon resonance (SPR) band at 420 nm. Figure 2 illustrates the formation of silver nanoparticles while adding AP extract and the concentration reaches 15µL the peaks start to disappear at 420nm due to electric attraction of metal particle accumulation.

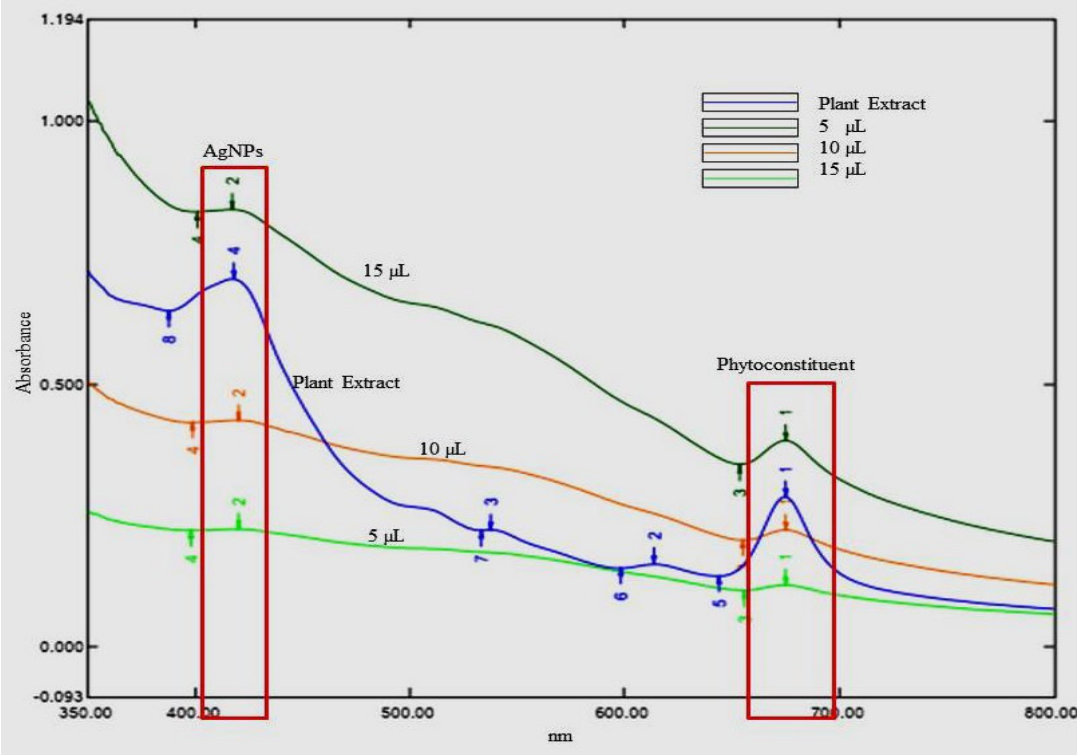

Figure 2. UV-visible spectrum of *Acalypha paniculata* silver nanoparticles.

The FT-IR spectra of the ethanolic extract, plain $AgNO_3$ solution, and synthesized nanoparticles of AP-AgNPs spectra were represented and compared in Figure 3a, 3b respectively. Initial interpretation analysis of AP phytoconstituents confirmed that the 15 phytoconstituents were present in the ethanolic extract. The IR spectral absorption shows that the broad and strong stretching peak appeared near the 3300 cm^{-1} (broad and strong) confirming the existence of -OH group-containing compounds. The peaks observed below the 3000 cm^{-1} (2970 cm^{-1} & 2885.51 cm^{-1}) proved that the sp3 C-H stretching groups contained compounds. The -C=C- stretching peaks appeared in the 1639.49 cm^{-1}, sp2 -C-O- peaks appeared at 1382.96 cm^{-1} and 1325.10 cm^{-1}. Di substituted aliphatic compounds developed the peaks at 881.47 cm^{-1}, 478.35 cm^{-1} to 389.62 cm^{-1} (Figure 3). The IR spectrum of prepared AP-AgNPs showed medium peaks of Alloaromadendrene at 1637.56 cm^{-1}. Biosynthesized Ag nanoparticle spectrum was compared with AP and $AgNO_3$ spectra.

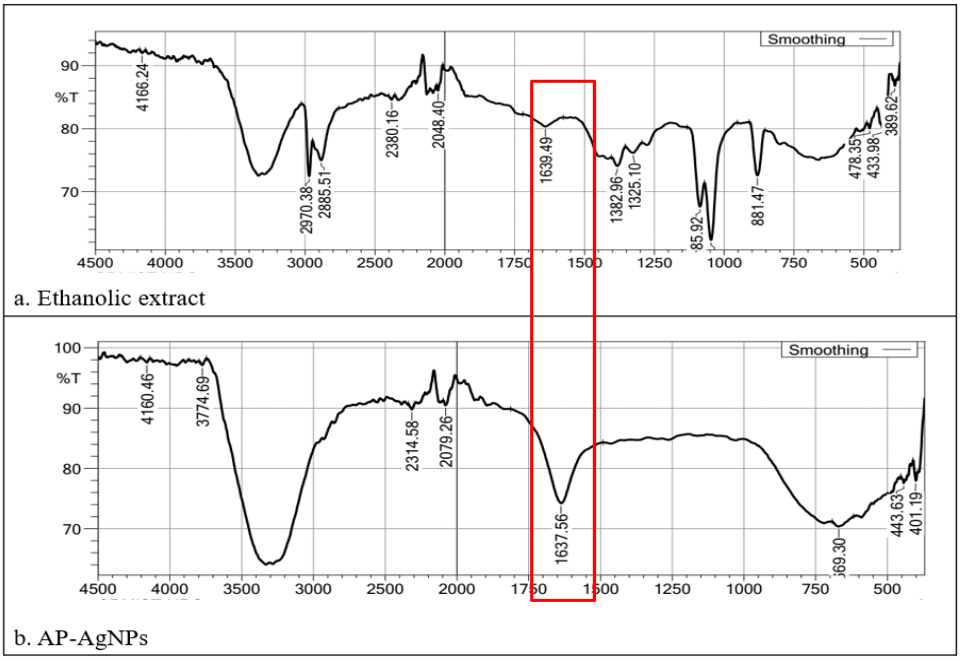

Figure 3. FTIR spectrum of *Acalypha paniculata* silver nanoparticles and silver ion peaks shown in red colour.

DLS and Zeta potential

The result of dynamic light scattering (DLS), gave the output hydrodynamic diameter of synthesised Ag nanoparticles in a suspension. Graphical figure of DLS measured the size of silver ion reduced by the AP extract and 94 % of the particles was 24.7 d.nm size and 54.7 d.nm of z-average with PDI score of 0.732 (Figure 4a). The colloidal stability of AgNPs was evidenced by a pronounced peak in the zeta potential distribution at –27.0 mV (Figure 4b).

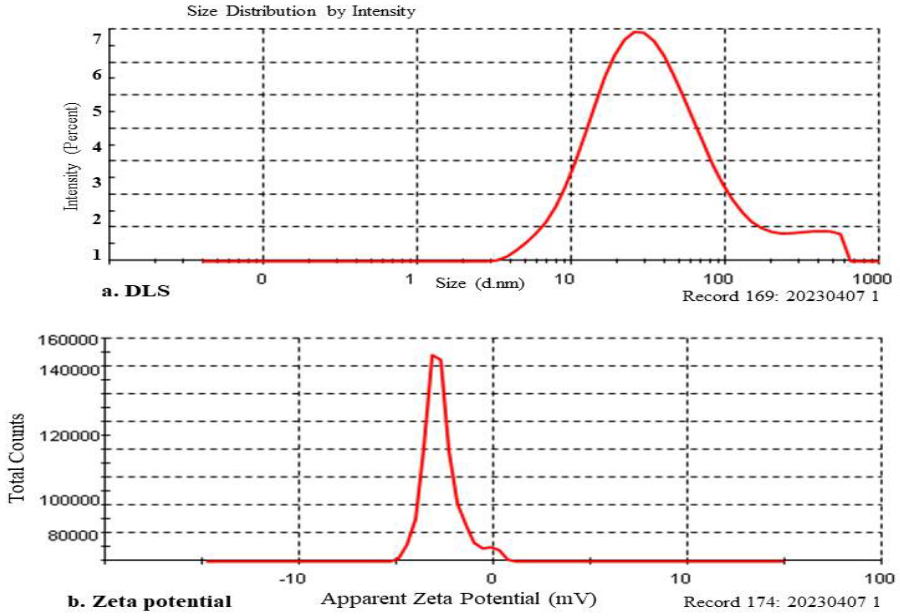

Figure 4. DLS (a). and Zeta potential (b). spectrum of *Acalypha paniculata* silver nanoparticles.

TEM

TEM provided detailed insights into the nanoparticle morphology; size and capping of phytoconstituents exhibited a size distribution ranging of 25-60 nm by over laying the given scale.

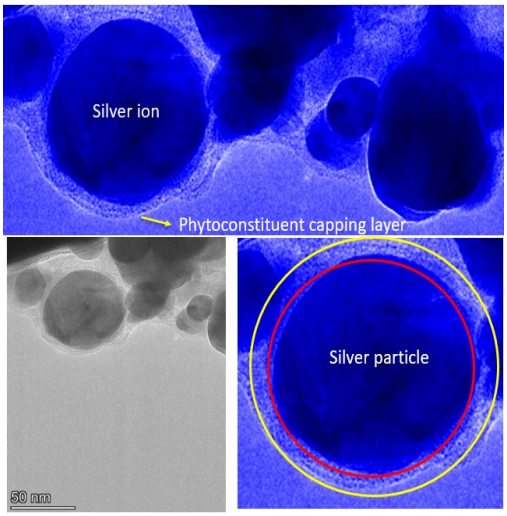

Figure 5. Transmission electron microscopy image of AP-AgNPs and its outer layer capping view.

Table 1. Size comparison table with TEM and DLS.

Particle size	TEM	DLS
Minimum	25 nm	24.7 nm
Maximum	60 nm	54.7 nm

X-ray diffraction (XRD)

The X-ray diffraction (XRD) pattern analysis affirmed the structural characteristics of the nanoparticles. It showcased peaks at 38.21°, 44.27°, 64.68°, and 77.59°, corresponding to the crystallographic planes of 111, 200, 220, and 311 respectively. These distinctive peak patterns are indicative of the crystalline nature of the silver nanoparticles, which were synthesized via the reduction of Ag+ ions. Thus, the XRD findings serve as compelling evidence for the crystalline structure of the synthesized silver nanoparticles.

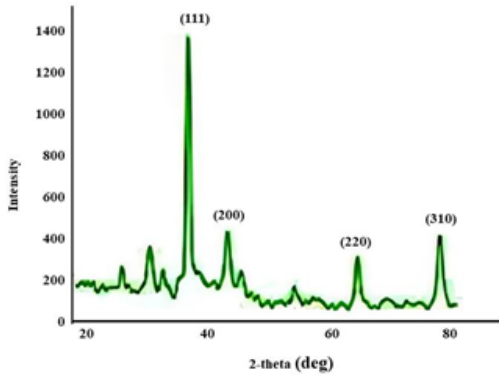

Figure 6. XRD spectrum of *Acalypha paniculata* silver nanoparticles Computational interaction of silver ion and phytoconstituents.

The forcite-steepest decent algorithm optimization reduces the energy of the phytoconstituent to the local minima level. Alloaromadendrene initial energy was reduced to -0.75580 kcal/mol from 331.9693 kcal/mol. Adsorption site analysis run protocol result exposed that the silver ion possible to form ionic interaction in the various sites of Alloaromadendrene. Specifically, the 11th carbon atom strongly attracts the silver ion and H38, H39, H22, and H20, possible to share the Vander Walls forces to form the interaction with Ag particle compared to nitrate ion as well as other 13 phytoconstituents.The adsorption energy of the silver ion-Alloaromadendrene complex was found to be -30.6755 kcal/mol.

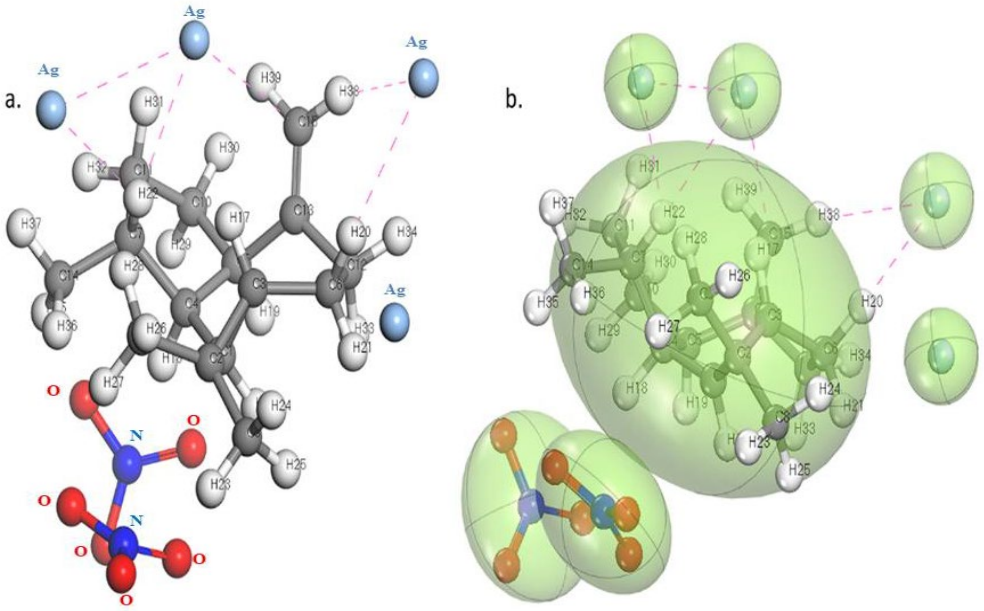

Figure 7. Silver nanoparticle interacting site with the Alloaromadendrene.

Antibacterial assay

The biogenic AgNPs displayed substantial growth inhibition against all tested microorganisms. The ranged from 22.67 ± 0.58 mm and 20.00 ± 0.00 mm for *Staphylococcus aureus* and *Bacillus cereus*, respectively. Similarly, the zone of inhibition was found to be 42.67 ± 0.58 mm and 30.00 ± 0.00 mm for *Escherichia coli* and *Pseudomonas fluorescens*, respectively (Figure 8). Clear zones of inhibition were seen surrounding the wells containing the AP-AgNPs in the agar plate, suggesting that the inhibition of bacterial growth. These zones of inhibition were larger and more pronounced compared to the ethanolic extract, where no nanoparticles were present. The standard antibiotic chloramphenicol was used as a reference for comparing the results of antimicrobial activity.

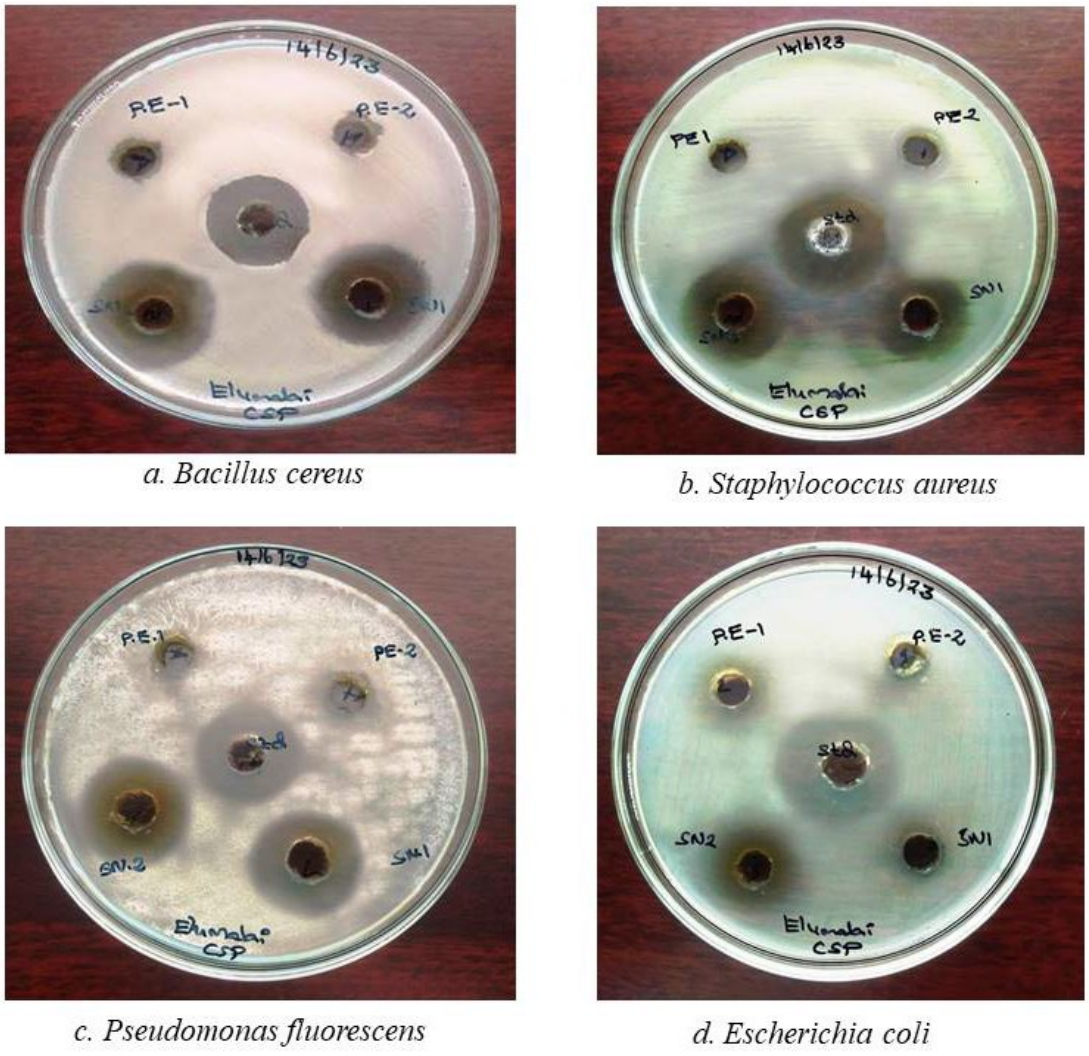

a. Bacillus cereus *b. Staphylococcus aureus*

c. Pseudomonas fluorescens *d. Escherichia coli*

Figure 8. Antibacterial assay of *Acalypha paniculata* silver nanoparticles.

DPPH Assay

In this study, the DPPH radical was tested at a concentration of 2mM against synthesized AP-AgNPs (silver nanoparticles) across various concentrations (50-1000 µg/ml). The investigation revealed a strong correlation between the incubation period and the radical scavenging activity of the silver nanoparticles, as depicted in Table 2. (IC_{50} 97.414). The high correlation coefficient (R=0.9925) of the linear regression (y=0.0428 x+49.476) indicates the appropriate linearity of the method. The extract exhibited a free radical scavenging activity equivalent to the control, indicating a noteworthy dosage-dependent relationship in its DPPH free radical scavenging capability.

Table 2. Antioxidant activity by DPPH.

Concentration (µg/ml)	Absorbance @517	%inhibition	IC_{50} =97.414
50	0.712	46.101	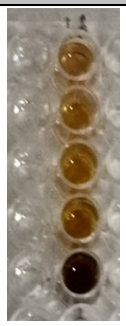
100	0.660	50.037	
250	0.597	54.806	
500	0.510	61.347	
1,000	0.439	66.704	

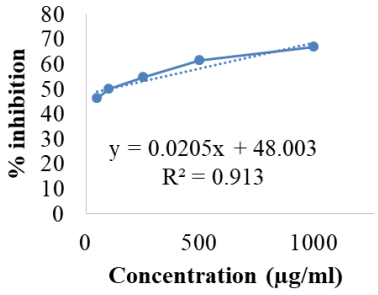

In-vitro cytotoxicity assay

Silver nanoparticles exhibit promising potential in the treatment of inflammation, as well as arthritic and cancer diseases. In order to validate and advance the development of anticancer formulations, the cytotoxicity of the synthesized AP-AgNPs was assessed in-vitro using the MTT assay on Vero cells. Subsequently, the corresponding IC_{50} values were calculated (Table 3). The absorbance value of AP-AgNPs was measured at 570 nm, indicating their distinctive viability in the normal cell line (Vero) in different concentrations of 1–512 µg/mL was observed and the IC_{50} was found to be 47.28 µg/mL.

The apoptotic morphological changes induced by AP-AgNPs were investigated using the acridine orange/ethidium bromide differential staining method. In this method, the stained cells were categorized into viable cells (light green), early apoptotic cells (bright green fluorescence with condensed chromatin), late apoptotic cells (orange fluorescence), and nonviable cells (red fluorescence) (Figure 8). The control group and AP-AgNPs exhibited intact green fluorescent cells with a well-organized structure. To the best of our knowledge, the present results correspond to the first report of the anticytotoxic activity of AP-AgNPs.

Table 3. Cytotoxicity activity of silver nanoparticles.

CONCENTRATION	PERCENTAGE OF VERO CELLS VIABILITY	
512	18.775 ± 6.084	
256	31.820 ± 4.835	
128	42.232 ± 5.174	

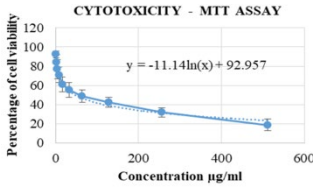

Table 3. Continued.

CONCENTRATION	PERCENTAGE OF VERO CELLS VIABILITY	
64	48.546 ± 6.477	
32	55.408 ± 7.635	
16	60.924 ± 7.608	
8	70.848 ± 7.914	
4	76.923 ± 9.956	
2	84.119 ± 7.594	
1	92.387 ± 3.485	

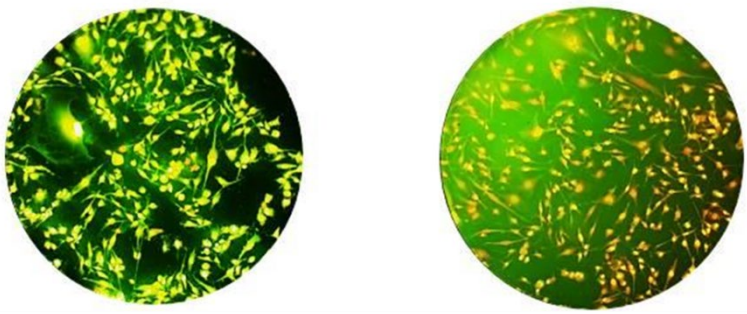

Figure 9. Apoptotic staining morphology of silver nanoparticles on Vero cells.

DISCUSSION

The color change in the formation of silver nanoparticles indicates the activation of Surface Plasmon Resonance, an interaction between light and metal nanoparticles (Ponsanti et al., 2020). The SPR peak observed at 420nm in UV-visible spectroscopy confirms the formation of silver nanoparticles, consistent with previous studies (Kalaiyan et al., 2023). Additionally, in FTIR spectra, an intense Alloaromadendrene is observed at 1637.56 cm^{-1}, indicating the reduction of silver ions to AgNPs. These spectral data provided evidence for the involvement of various categories of phytoconstituents, including alkaloids, sesquiterpenes, phenols, and saponins, in the synthesis of silver nanoparticles (Wang et al., 2021).

DLS analysis revealed that the AP extract reduced the size of silver ions, with 94% of the particles measuring an average of 54.7 nm, yielding a PDI score of 0.732. The colloidal stability of the AgNPs was indicated by a prominent peak in the zeta potential distribution at -27.0 mV. Both DLS and the observed zeta potential highlighted effective electrostatic repulsion among the nanoparticles, mitigating aggregation caused by van der Waals attractive forces. Additionally, TEM images confirmed the quasi-spherical shape of the nanoparticles, providing further evidence of their morphology (Sheik Aliya et al., 2023).

According to Khan et al., (2023) XRD analysis revealed a peak at 38.21°, indicating the presence of pure silver nanoparticles. Furthermore, X-ray diffraction investigations specified that these AP-AgNPs were crystalline in nature.

Computational studies revealed the presence of van der Waals (vdW) attraction forces between the silver ion and Alloaromadendrene, involving the nitrate ions. This findings affirm the capping of Alloaromadendrene on the silver ion, playing a role in the fabrication of nanoparticles (Irfan and Puratchikody, 2012).

Previous studies have also reported the antibacterial activity of AgNPs against gram-negative and gram-positive strains of bacteria. The antibacterial effect of AgNPs is well-recognized to be size and dose-dependent (Shivananda et al., 2016; Kindnew Demssie Dejen et al., 2023; Shivananda et al., 2023). The diverse mechanisms that consider the physicochemical properties of AgNPs, including size and surface characteristics. These properties enable AgNPs to interact with, and potentially penetrate, cell walls or membranes, directly influencing intracellular components. Our study demonstrated that AP-AgNPs potentially inhibited the growth of both gram-positive and gram-negative bacteria, when used in very low concentrations. Furthermore, the synergistic anti-bacterial effects of the AP-AgNPs may result from the capping of phytoconstituents with silver nanoparticles (Musa et al., 2000).

AgNPs encounter DPPH (2,2-diphenyl-1-picrylhydrazyl) radicals, they undergo a reduction reaction, donating electrons to the DPPH radicals and thereby neutralizing their unpaired electron, resulting in the formation of stable DPPH molecules. This process effectively scavenges the free radicals, thereby exhibiting antioxidant activity. (Khojasteh-Taheri et al., 2023). The observed effect of different concentrations of AP-AgNPs on DPPH radical antioxidant activity is dose-dependent, as shown in Table 2. The IC_{50} value of 97.414 demonstrates the presence of strong antioxidant activity comparable to the standard ascorbic acid.

The synthesized AgNPs were further tested to evaluate their cytotoxicity effect on Vero cells. Dose-dependent cell toxicity was observed at a high concentration of AP-AgNPs (128 µg/mL), and the IC_{50} was found to be 47.28 µg/mL. AgNPs indicated no detrimental impacts on the Vero cell line as stated by various researchers. (Jamil et al., 2022; Shater et al., 2023; Huda Abd Kadir

et al., 2024). These results also support the previous findings which showed less cell toxicity and more cell proliferation.

The viability of Vero cells was confirmed by the Acridine Orange/Ethidium Bromide differential staining method, and the results exhibited green fluorescent cells, indicating non-toxicity in Vero cells.

Disadvantages

Silver nanoparticles (AgNPs) produced in medicinal plants offer several advantages, such as their potential antimicrobial and therapeutic properties. However, they also come with certain disadvantages like Biocompatibility concerns, Contamination risk, Standardization challenges, Potential toxicity, Environmental impact, Regulatory considerations. Overall, while AP-AgNPs produced in medicinal plants hold promise for various biomedical applications, careful assessment of their advantages and disadvantages is necessary to harness their potential effectively while mitigating associated risks.

CONCLUSION

This research showcases the utilization of *Acalypha paniculata* leaves to establish an innovative and efficient approach for synthesizing silver nanoparticles. The method devised is characterized by its simplicity, speed, and affordability, as it involves a single-step process. The synthesis process encompasses both the stabilization of the nanoparticles and the reduction of silver ions. Previous studies reported that this plant contains pyridine alkaloids, flavonoids, and terpenoids, which contribute to the nanoparticle synthesis process. Finally, these AP-AgNPs demonstrated notable antibacterial activity against various gram strains and cytotoxicity against Vero cells, indicating their potential as safe and effective medicine.

ACKNOWLEDGEMENTS

Authors are thankful to Crescent School of Pharmacy for providing necessary facilities for carried out of this research.

AUTHOR CONTRIBUTIONS

Mr. A Elumalai performed all the works and the Dr Irfan N conceptualised and framed the article.

CONFLICT OF INTEREST

The authors report no conflicts of interest. The authors alone are responsible for the content and writing of this article.

ETHICAL STATEMENT

Neither ethical approval nor informed consent was required for this study.

REFERENCES

Djacbou D, S., Pieme C, A., Biapa P, C., and Penlap B, V. 2014. Comparison of *in vitro* antioxidant properties of extracts from three plants used for medical purpose in Cameroon, *Acalypha racemosa, Garcinia lucida* and *Hymenocardia lyrata.* Asian Pacific Journal of Tropical Biomedicine. 4(2): S625-S632.

Eli, R. and Anna, R. 2022. Application of silver nanoparticles synthesized by using *Ipomoea batatas* L. waste to improve antibacterial properties and hydrophobicity of polyester cloths. Chiang Mai Journal of Science. 45(7): 2715-2729.

Flieger, J., Wojciech, F., Rafał, P., Monika S, C., Wojciech, F., Michał, F., and Przemysław, K. 2021. Green synthesis of silver nanoparticles using natural extracts with proven antioxidant activity. Molecules. 26(16): 4986.

Gunashekar K, S., Susmila A, G., Venkata S, K., Hema G., Sashikiran P., Josthna P., and Varadarajulu N, C. 2023. Green fabrication of silver nanoparticles by leaf extract of *Byttneria herbacea* Roxb and their promising therapeutic applications and its interesting insightful observations in oral cancer. Artificial Cells, Nanomedicine and Biotechnology. 51(1): 83-94.

Hafiz S, A., Muhammad, A., Sobia, N., Muhammad I, F., Mirza M, F., Ashraf, B., Muhammad S, N., Muhammad, F, A, Khalil, A., Ali, R.A., Hina, S., Faheem, H., and Asadullah, M. 2023. Biomimetic synthesis and characterization of silver nanoparticles from *Dipterygium glaucum* extract and its anti-cancerous activities. Journal of Molecular Structure. 1282: 135196.

Huda Abd Kadir, N., Ali Khan, A., Kumaresan, T., Khan, A.U., and Alam, M. 2024. The impact of pumpkin seed-derived silver nanoparticles on corrosion and cytotoxicity: A molecular docking study of the simulated AgNPs. Green Chemistry Letters and Reviews, 17(1): 2319246.

Iniaghe O, M., Malomo S, O., Adebayo J, O., and Arise R, O. 2008. Evaluation of the antioxidant and hepatoprotective properties of the methanolic extract of *Acalypha racemosa* leaf in carbon tetrachloride-treated rats. African Journal of Biotechnology. 7: 1716-1720.

Irfan, N. and Puratchikody, A. 2019. Identification of silver nanoparticle-shaping tridax procumbens phytoconstituent by theoretical simulation and experimental correlation. Indian Journal of Pharmaceutical Science. 81(5): 900-912.

Khojasteh-Taheri, R., Ghasemi, A., Meshkat, Z., Sabouri, Z., Mohtashami, M., and Darroudi, M. 2023. Green synthesis of silver nanoparticles using *Salvadora persica* and *Caccinia macranthera* extracts, cytotoxicity analysis and antimicrobial activity against antibiotic-resistant bacteria. Applied Biochemistry and Biotechnology. 195(8): 5120-5135.

Kindnew D, D., Desalegn Y, K., Tadesu H, M., Eneyew T, B., Abebe T., Temesgen A, B., and Fikade T, D. 2023. Green synthesis and characterisation of silver nanoparticles from leaf and bark extract of *Croton macrostachyus* for antibacterial activity. Materials Technology. 38(1): 2164647.

Kalaiyan G., Prabu K, M., Suresh, N., and Suresh, S. 2023. Green synthesis of copper oxide spindle like nanostructure using *Hibiscus cannabinus* flower extract for antibacterial and anticancer activity applications. Results in Chemistry. 5: 100840.

Linima R., R. and Jesteena J., R. 2023. Biogenic synthesis of Ricinus communis mediated iron and silver nanoparticles and its antibacterial and antifungal activity, Heliyon. 9(5): e15743.

Luhata, L.P., Chick, C.N., Mori, N., Tanaka, K., Uchida, H., Hayashita, T. and Usuki, T. 2022. Synthesis and antioxidant activity of silver nanoparticles using the *Odontonema strictum* leaf extract. Molecules. 27: 3210.

Jamil K., Khattak SH., Farrukh A., Begum S., Riaz MN., Muhammad A., Kamal T., Taj T., Khan I, Riaz S., et al. 2022. Biogenic synthesis of silver nanoparticles using *Catharanthus roseus* and its cytotoxicity effect on vero cell lines. Molecules. 27(19):6191.

Khan, J., Naseem, I., Bibi, S., Ahmad, S., Altaf, F., Hafeez, M., Almoneef, M.M., and Ahmad, K., 2023. Green synthesis of silver nanoparticles (Ag-NPs) Using *Debregeasia salicifolia* for biological applications. Materials. 16(1): 129.

Musa K., Y., Ahmend, A., Ibrahim, H., Arowosiaye, G., Olanitola, O., S. 2000. Phytochemical and antibacterial studies of leaves of *Acalypha racemosa*. Nigerian Journal of Natural Products and Medicine. 4: 67-69.

Ponsanti, K., Benchamaporn, T., Nipaporn, N., Chiravoot, P. 2020. A flower shape-green synthesis and characterization of silver nanoparticles (AgNPs) with different starch as a reducing agent. Journal of Market Research. 9(5): 11003–11012.

Sarinya P., Niti Y., and Siriporn P. 2017. Synthesis, characterization, and antibacterial properties of silver nanoparticles prepared from aqueous peel extract of pineapple, *Ananas comosus*. Chiang Mai University Journal of Natural Sciences. 16(2): 123-133.

Shater A., Saleh F., Mohammedsaleh Z., Gattan H., Al-Ahmadi B., Saeedi N., Jalal M., Panneerselvam C. 2023. Green nanoarchitectonics of the silver nanocrystal potential for treating malaria and their cytotoxic effects on the kidney Vero cell line. Green Processing and Synthesis. 12(1): 20228111.

Sheik A., Muruganantham R., Jingon Y., Eunsu K., Joo Y. C., Jong H, C., and Yun S, H. 2023. Phytogenic fabrication of iron oxide nanoparticles and evaluation of their *in vitro* antibacterial and cytotoxic activity. Arabian Journal of Chemistry. 16(6): 104703.

Shivananda C.S., Lakshmeesha Rao B., Azmath Pasha, and Y Sangappa. 2016. Synthesis of silver nanoparticles using *Bombyx mori* silk fibroin: Their characterization and antibacterial activity. IOP Conference Series: Material Science and Engineering. 149: 012175.

Shivananda C.S., 2023. Silk fibroin-based green colloidal silver nanoparticle synthesis and their antibacterial and anticancer properties. Inorganic Chemistry Communications. 158(2): 111611.

Usa S., Awadol K., Phitsamai K., Anuchit R., Sirichatnach P and Pornprapa K. 2023. Biosynthesis of silver nanoparticles using *Garcinia cowa* aqueous leaf extract and their antifungal activity against durian dieback pathogen. Chiang Mai Journal of Science. 50(5): 1-14.

Vanlalveni, C., Lallianrawna, S., Biswas, A., Selvaraj, M., Changmai, B., and Rokhum, S.L. 2021. Green synthesis of silver nanoparticles using plant extracts and their antimicrobial activities, A review of recent literature. RSC Advances. 11: 2804–2837.

Wang Y., Arunachalam C., Omaima N., and Sulaiman A. A. 2021. Green synthesis and chemical characterization of a novel anti-human pancreatic cancer supplement by silver nanoparticles containing *Zingiber officinale* leaf aqueous extract. Arabian Journal of Chemistry. 14: 103081.

OPEN access freely available online
Natural and Life Sciences Communications
Chiang Mai University, Thailand. https://cmuj.cmu.ac.th